Ultrafast formation of a transient two-dimensional diamondlike structure in twisted bilayer graphene

Duan Luo,[1,2,3] Dandan Hui,[2,3] Bin Wen,[4] Renkai Li,[5,*] Jie Yang,[5] Xiaozhe Shen,[5] Alexander Hume Reid,[5] Stephen Weathersby,[5] Michael E. Kozina,[5] Suji Park,[5] Yang Ren,[6] Troy D. Loeffler,[1] S. K. R. S. Sankaranarayanan,[1] Maria K. Y. Chan,[1] Xing Wang,[2] Jinshou Tian,[2,7] Ilke Arslan,[1] Xijie Wang,[5] Tijana Rajh,[1,†] and Jianguo Wen[1,‡]

[1]*Center for Nanoscale Materials, Argonne National Laboratory, Lemont, Illinois 60439, USA*

[2]*Key Laboratory of Ultra-fast Photoelectric Diagnostics Technology, Xi'an Institute of Optics and Precision Mechanics, Chinese Academy of Sciences, Xi'an 710119, China*

[3]*University of Chinese Academy of Sciences, Beijing 100049, China*

[4]*State Key Laboratory of Metastable Materials Science and Technology, Yanshan University, Qinhuangdao 066004, China*

[5]*SLAC National Accelerator Laboratory, Menlo Park, California 94025, USA*

[6]*X-ray Science Division, Argonne National Laboratory, Lemont, Illinois 60439, USA*

[7]*Collaborative Innovation Center of Extreme Optics, Shanxi University, Taiyuan 030006, China*

(Received 18 March 2020; accepted 5 October 2020; published 29 October 2020)

Due to the absence of matching carbon atoms at honeycomb centers with carbon atoms in adjacent graphene sheets, theorists predicted that a sliding process is needed to form *AA*, *AB′*, or *ABC* stacking when directly converting graphite into sp^3 bonded diamond. Here, using twisted bilayer graphene, which naturally provides *AA* and *AB′* stacking configurations, we report the ultrafast formation of a transient two-dimensional diamondlike structure (which is not observed in aligned graphene) under femtosecond laser irradiation. This photoinduced phase transition is evidenced by the appearance of bond lengths of 1.94 and 3.14 Å in the time-dependent differential pair distribution function using MeV ultrafast electron diffraction. Molecular dynamics and first-principles calculation indicate that sp^3 bonds nucleate at *AA* and *AB′* stacked areas in a moiré pattern. This work sheds light on the direct graphite-to-diamond transformation mechanism, which has not been fully understood for more than 60 years.

DOI: 10.1103/PhysRevB.102.155431

Atomically thin twisted van der Waals (vdW) materials with a rotational misalignment introduce a moiré pattern [1–11], leading to intriguing electronic properties such as unconventional superconductivity [2,3] and correlated insulating states [4] by modulating the band structure of the material. New optical phenomena such as moiré excitons [5–8] in vdW heterostructures were also reported at different twisted angle configurations. Meanwhile, optical control of structural and electronic properties, especially through photoinduced phase transition (PIPT), has recently attracted tremendous attention due to its great potential in functionalization of two-dimensional (2D) materials [12–16]. A detailed study of the changes in bonding network and the resulting metastable dynamics triggered by photoexcitation is necessary but challenging since it's an intrinsically out-of-equilibrium process [17]. These make the ultrafast probing of the fundamental light-matter interactions in twisted 2D vdW materials, especially twisted bilayer graphene (TBG), very attractive.

In perfectly aligned graphene structures with *AB* stacking, the absence of matching carbon atoms at honeycomb centers with carbon atoms in adjacent layers hinders direct transformation into diamond. Therefore, extensive theoretical research suggests that the direct transformation from hexagonal graphite to diamond must undergo a sliding process to *AB′* stacking [18], *AA* stacking [19], or *ABC* stacking [20] configurations, followed by boat or chair buckling (see Fig. S1 of the Supplemental Material [21]). On the other hand, TBG naturally creates a moiré pattern with periodic metastable *AA* and *AB′* stacked local areas [Figs. 1(a) and 1(b)]. Upon excitation, these areas are expected to easily form sp^3 rich metastable structures [Fig. 1(c)]. We chose an fs laser to initiate the structural phase transition, since it has been demonstrated that fs laser irradiation has the ability to convert graphite to diamond structure at ambient temperature and pressure [22–24]. When excited by an intense laser pulse, nonequilibrium carriers are generated and the resulting electron-hole plasma which consists of electrons and holes in distinct graphene layers will induce a strong electrostatic force between graphene layers and contract the interlayer distance. Moreover, the interlayer separation will be also reduced by the photoexcitation-induced charge density changes which modify the force field in the bonding system and increase the interlayer attraction [25]. Such a scenario in graphite has been reported by different groups [24–27], for example, Nasu *et al.* [24] identified a photoinduced nanostructure consisting of a mixed sp^2-sp^3 hybridization (named diaphite) by scanning tunneling microscopy. Additionally, ultrashort laser

*Corresponding author: lrk@slac.stanford.edu
†Corresponding author: rajh@anl.gov
‡Corresponding author: jwen@anl.gov

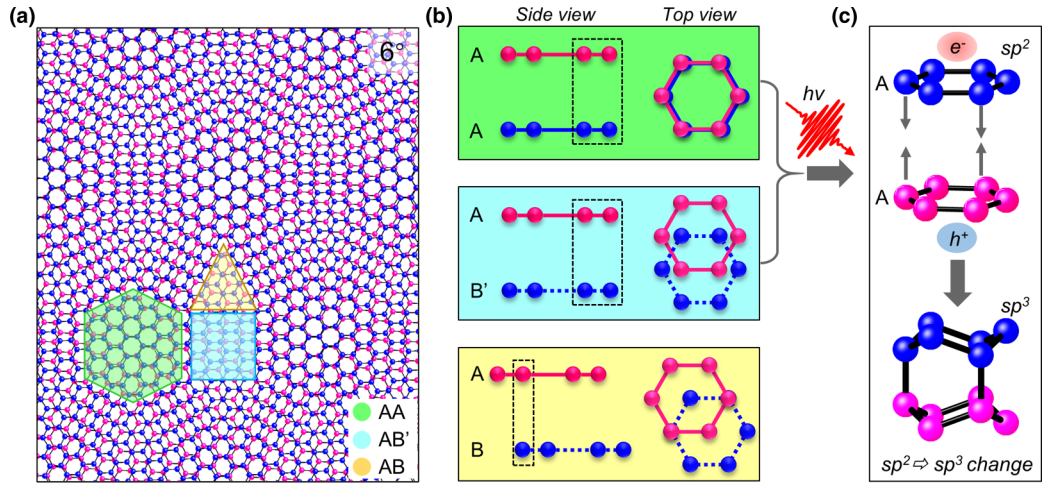

FIG. 1. Photoinduced structural transition from twisted bilayer graphene (TBG) to 2D diamond structure. (a) Schematic of a TBG moiré pattern at 6°, which consists of regions with *AB*, *AA*, and *AB′* stackings as structural details shown in (b). (c) Schematic illustration of the photoinduced structural transition in TBG, taking *AA* stacking as an example. Subsequent to the fs laser irradiation, interlayer contraction and buckling are induced by the generated electron-hole plasma which consists of electrons and holes in distinct graphene layers and then the transformation of sp^2 bonds to sp^3 bonds occurs. Such a transformation occurs preferentially at regions with *AA* and *AB′* stacking rather than at *AB* stacked areas due to the lack of matching carbon atoms at honeycomb centers between adjacent *AB* stacked graphene layers [top view in (b)].

excitation can be coupled with an ultrafast electron pulse in a pump-probe configuration to enable the study of the structural dynamics in real time [25,26]. Ultrafast electron diffraction (UED) systems in the reflection and transmission geometry have been successfully used to investigate the out-of-plane and in-plane lattice dynamics of graphite [26–31] and monolayer graphene [32], respectively. In reflection-mode studies, graphite undergoes an initial compression and then a successive expansion along the *c* axis [26,27]. At higher fluences approaching the damage threshold, a transient sp^3-like structure was reported by Raman *et al.* [25]. Since transient electric fields generated by photoexcitation may interfere with structural dynamics by deflecting the electron packets [33–35], excluding such effects in these surface diffraction studies is extremely challenging. In transmission-mode studies, graphite shows a biexponential Debye-Waller-like behavior with sub-ps and sub-10 ps time scales [28–30] due to the incoherent coupling of ultrafast electronic excitation to the strongly coupled optical-phonon modes and the following relaxation processes. Besides the incoherent coupling, strong coherent oscillation (shear and breath mode) was observed through the coherent coupling of the photoexcitation to lattice motions [29].

Here we report the photoinduced sp^2-sp^3 transformation in TBG where the moiré pattern plays an important role. Through analysis of the differential pair distribution function (ΔPDF), an ultrafast formation of diaphitene from TBG was observed after fs laser irradiation. Similar to its corresponding bulk form (called diaphite [24,36]), diaphitene exhibits interlayer sp^3 bonding but differs from a diamond lattice with C-C bond length of 1.54 Å. Furthermore, the recorded dynamics revealed that the transition was completed within 330 fs and the structure was maintained as diaphitene for at least 2 ns and eventually recovered back to the graphene structure within 5.56 ms (pump frequency 180 Hz).

Large area TBG samples were prepared by stacking two chemical vapor deposition (CVD) monolayer graphene sheets on gold grids with a holey carbon support film (see Supplemental Material [21]). Each graphene sheet in TBG consists of numerous grains with a typical grain size of ∼5 μm. Twist angles are determined from 137 different overlapped domains using selected-area electron diffraction (SAED) with a 500-nm aperture to be a broad distribution concentrated at ∼ 12° (see Fig. S2 of the Supplemental Material [21]). Through analysis of the intensity profile along the green line marked in the SAED pattern, we can determine that almost all the areas are stacked by two-monolayer graphene since the intensity ratios $I_{\{100\}}/I_{\{110\}} > 1$ [37]. UED experiments were performed using an electron pulse (∼120-μm probe size, ∼130 − fs pulse length) at normal incidence. The UED diffraction pattern of TBG consists of Debye-Scherrer rings [Fig. 2(a)], since the grain size in TBG (∼ 5 μm) is much smaller than the probe size of the electron pulse (∼ 120 μm). The time-dependent intensity of {100} and {110} diffraction rings after photoexcitation at an incident fluence of ∼9.7 mJ/cm^2 is shown in Fig. 2(b). Similar phenomena were also observed at a fluence of ∼4.2 mJ/cm^2 (Fig. S3 of the Supplemental Material [21]). The intensity changes clearly show an initial ultrafast component followed by a slower one. The time evolution was thus fitted by biexponential functions $\frac{\Delta I}{I_0}(t) = A(1 - e^{-t/\tau_1}) + B(1 - e^{-t/\tau_2})$. The extracted time constants are $\tau_1 = 115$ fs and $\tau_2 = 585$ fs for the {100} peak and $\tau_1 =$ 188 fs and $\tau_2 = 10.8$ ps for the {110} peak (Fig. S3 [21]), respectively. Such a rapid intensity rise in the {100} peak and a drop in the {110} peak indicate that this process is not a thermal effect (since an increase in the temperature enhances random atomic thermal vibration, resulting in a drop of *all* Bragg peaks' intensities), but possibly induced by in-plane buckling during interlayer contraction (Fig. S4 [21]). This can be further supported by the following Q shift and ΔPDFs.

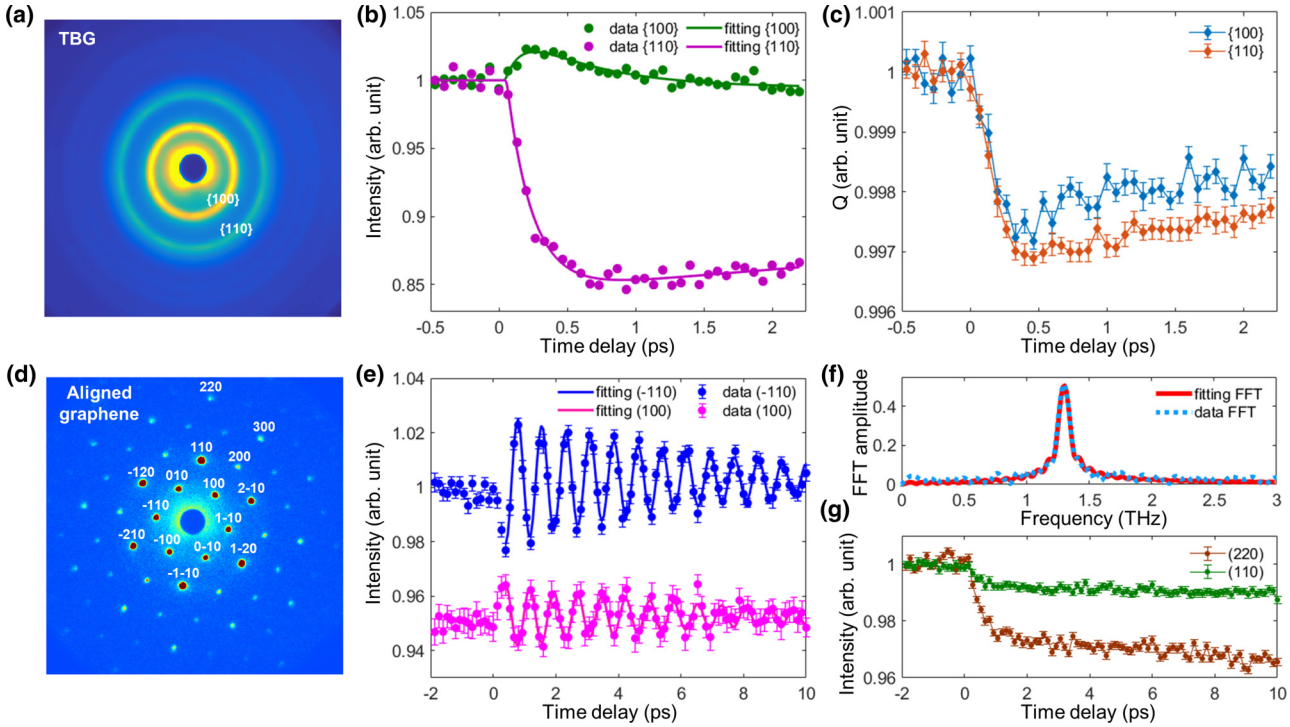

FIG. 2. Ultrafast structural dynamics in twisted bilayer graphene (TBG) (upper row) and aligned graphene layers (lower row). (a) Typical diffraction pattern of TBG observed by MeV UED, labeled the first two most visible rings ({100} and {110}). (b) Diffraction intensity changes as a function of time delays. A rapid intensity rise in the {100} and drop in the {110} indicate that this process is not a thermal effect. (c) Time-dependent Q shift of TBG showing the ultrafast structural transformation within 330 fs (from {100}). (d) Typical diffraction pattern of aligned graphene sheets observed by MeV UED. (e) Oscillatory dynamics in {100} family showing out-of-phase shear mode vibration between (−110) and (100) peaks. (f) Extracted modulation frequency. (g) Q-dependent peak intensity decay.

The temporal evolution of the magnitude of the momentum transfer vector Q (i.e., $Q = \frac{2\pi}{d_{hkl}}$) is illustrated in Fig. 2(c). Both the {100} and {110} peaks shift to a lower Q within ∼330 fs. Photoinduced electron-phonon and phonon-phonon scattering which heats the lattice and results in thermal expansion can also result in an increase of lattice spacing. However, graphene sheets have a negative in-plane thermal-expansion coefficient [38], i.e., they contract when heated and the lattice expansion in graphene due to the excitation of in-plane acoustic-phonon modes happens at a longer time scale of 5 ps [32]. The observed reduction in Q within ∼330 fs (increase in the in-plane lattice spacing) indicates a possible conversion of graphene sheets into a hexagonal diamond (HD)-like structure [Fig. 2(c)], since the lattice spacings in HD [2.18 Å (100) and 1.26 Å (110)] is larger than that in graphene sheets [2.13 Å (100) and 1.23 Å (110)]. Repeated pump-probe experiments show that the change is reversible, but it does not revert to graphene even after ∼2 ns as shown in the long-runtime experiment (Fig. S3 [21]). To rule out the possible contribution due to the supporting amorphous carbon (AC) film, we performed ultrafast experiments on the AC film. No obvious changes occurred in time-dependent Q of the AC films compared to the TBG (Fig. S3 [21]), thus confirming that the structural transformation is truly from the TBG.

For clear comparison of an ultrafast structural transformation in aligned bilayer and few-layer graphene, we carried out UED experiments on free-standing *AB*-stacked aligned bilayer and few-layer graphene (Fig. S5 [21]) under the same conditions. We found that there are no noticeable changes in time-dependent Q compared to TBG (Fig. S6 [21]); i.e., no phase transitions occur in aligned graphene sheets. Instead, the {100} diffraction peaks of aligned graphene sheets exhibit a strong out-of-phase shear mode vibration with a clear oscillation period of 0.8 ps and a damping time of 15 ps [Fig. 2(e)], similar to the results reported by Siwick *et al.* [29]. We further obtained a shear mode frequency of ∼1.3 THz [Fig. 2(f)] for aligned graphene sheets by Fourier transforming the coherent vibration [Fig. 2(e) and Fig. S6 [21]]. This measured frequency is in good agreement with the Γ-point transverse optical-phonon mode which can explain the above out-of-phase relationship by modeling the time-resolved structure factor [29]. A drop in intensities with time delays was observed in the high-order {110} and {220} peaks [Fig. 2(g)]. Even doubling the fluence to ∼19 mJ/cm^2 showed no other changes except a larger amplitude (Fig. S6 [21]).

MeV electrons enable UED from TBG to satisfy a kinematic approximation similar to the ones used in x-ray and neutron diffraction. Therefore, the time-dependent ΔPDF [39] was calculated from the diffraction patterns to further extract the structural dynamics of TBG following photoexcitation. The diffraction-difference method which employs the subtraction of diffraction signals before and after optical excitation was used to highlight these changes (see the Supplemental Material [21]). The experimental ΔPDF (at fluence of ∼9.7 mJ/cm^2) as a function of the pump-probe time delay between −200 and 1000 fs with a step size of 67 fs is shown

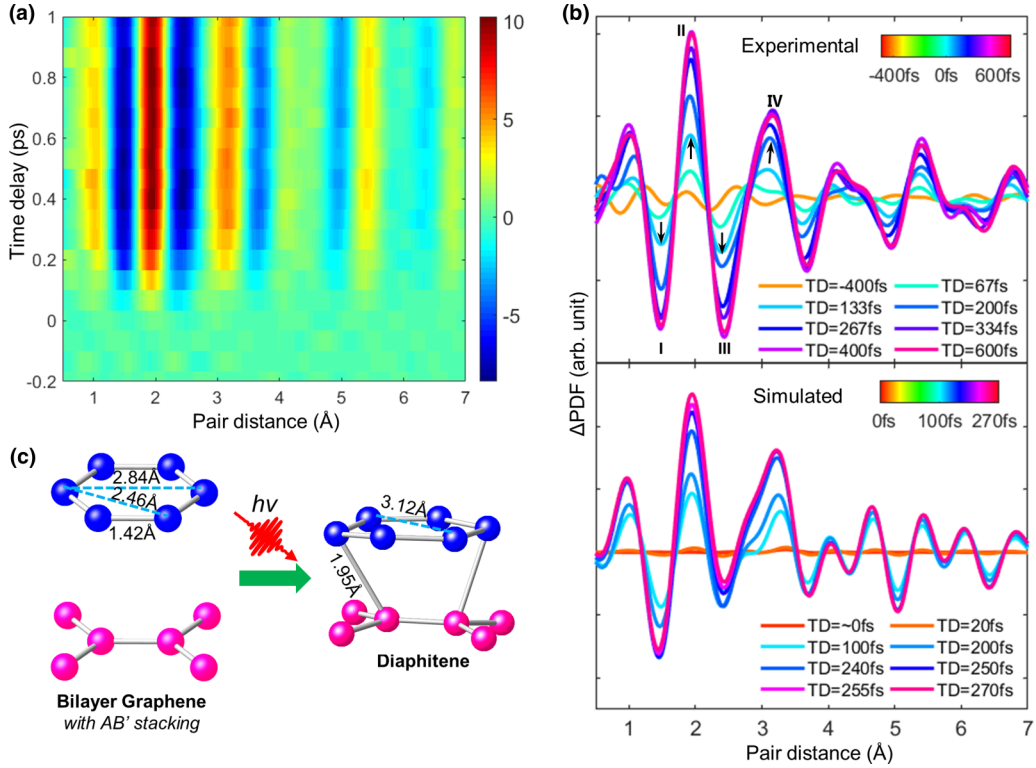

FIG. 3. Temporal evolution of difference pair distribution functions (ΔPDF). (a) Experimental 2D ΔPDF of twisted bilayer graphene (TBG) showing the intensity increase (warm color) and decrease (cool color) at different interatomic distances and different time delays. (b) One-dimensional experimental and simulated ΔPDF at different time delays. The observed reduction of 1.42 Å (I) and 2.46 Å (III) bonds in (b) matches with the bonds in graphene (c) before the transformation. The appearance of 1.94 Å (II) and 3.14 Å (IV) bonds observed in TBG matches the new diaphitene structure (c) extracted from simulated transient structures (Fig. S9 [21]).

in Fig. 3(a), with blue indicating loss and red indicating gain in the ΔPDF at various atom pair distances compared with unexcited TBG. Ultrafast changes in interatomic distances were observed from the ΔPDF. By choosing the appropriate time delays [from Fig. 3(a) and Fig. S7 [21]], we obtained a series of one-dimensional ΔPDFs, as shown in Fig. 3(b). The positive peaks (II, IV) represent a significant increase in the ΔPDF at interatomic distances r of 1.94 and 3.14 Å, while the negative peaks (I, III) correspond to a reduction of the ΔPDF at interatomic distances at 1.42 and 2.46 Å [Fig. 3(b)]. The ultrafast bond length distribution changes reach a maximum at 330 fs (Fig. S7 [21]). The static PDF of graphene sheets studied by x-ray and neutron diffraction [40,41] shows three nearest-neighbor pair distances in the honeycomb graphene lattice: 1.42, 2.46, 2.84 Å [Fig. 3(c), Fig. S8 [21]]. When compressing two graphene layers to an interlayer distance d, the PDF with pair distances $<d$ has the contribution only from monolayer graphene regardless of twist angles and stacking sequences [40,41]. In other words, the appearance of new bond lengths other than 1.42, 2.46, 2.84 Å in the PDF reflects that the interlayer distance is reached to the smallest valve of new bond lengths. Therefore, the observation of new bonding distances of 1.94 and 3.14 Å indicates the ultrafast formation of interlayer sp^3 bonds after the fs laser irradiation [Fig. 3(c)].

To understand the detailed structural evolution during compression, we carried out molecular dynamics (MD) simulations for TBG with different twist angles (0°, 6°, 12°, 18°, and 30°) (see the Supplemental Material [21]). All TBGs with twist angles other than 0° with *AB* stacking showed similar structural dynamics (Fig. S9 [21]). Taking a typical angle of 12° as an example (the approximate center angle in our experimental work), one can see that after excitation, sp^3 bonds labeled with red and orange (warm colors) are preferentially formed in local areas with stacking close to *AA* and *AB′*, but almost no sp^3 bonds are formed (shown in blue) in the area with *AB* stacking from the top-view snapshots [Fig. 4(a) and Fig. S9 [21]]. These simulation results support our experimental observations of ultrafast phase transitions in TBG but not in aligned graphene sheets that are composed entirely of the *AB* stacking configuration. The reversible phase transition occurs within ~270 fs, but it takes a much longer time to recover due to the strong covalent interaction of C-C bonds between two graphene layers as shown in the side-view and perspective-view snapshots [Fig. 4(b), Fig. S9 [21]]. This explains why the structural change occurs within 330 fs and remains in the transient state longer than 2 ns.

Using the simulated transient structures, we calculated their ΔPDFs by selecting several representative moments (Fig. S9 [21]). These calculated ΔPDFs match well with the experimental ones [Fig. 3(b)], although there is a slight difference above 4 Å between the experimental and the simulated ΔPDF. This difference may be caused by distribution of various twist angles in experimental TBG. From the transient TBG structure at the time of ~270 fs with maximum numbers of sp^3 bonds, a new transient state [Fig. 3(c)] is extracted, which explains the emergence of new pair distances

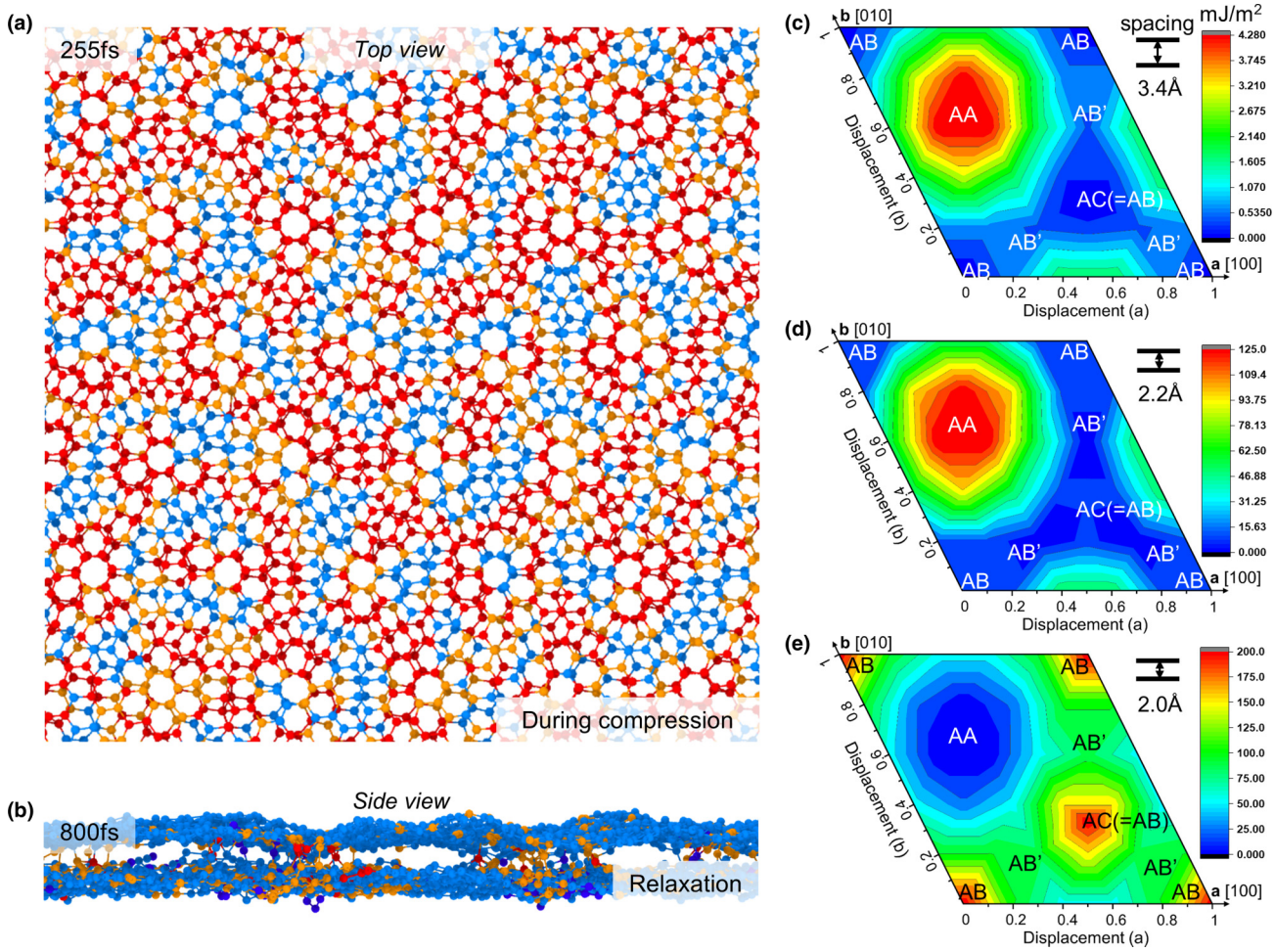

FIG. 4. Simulated structural evolution and energy pathway. (a) Snapshot of the top view at 255 fs (during compression) showing the preferential formation sp^3 bonds (warm colors) at regions with *AA* and *AB*′ stacking. (b) Snapshot of the side view at 800 fs showing the strong interlayer C-C bonds slow down the relaxation. (c)–(e) Generalized stacking fault energy surfaces for interlayer spacing of 3.4, 2.2, and 2.0 Å. When the layer spacing is compressed from 3.4 to 2.0 Å, the lowest free-energy configuration gradually changes from *AB* stacking (c) to *AB*′ (d) and *AA* (e) stacking. This 2D map of bilayer graphene with different stacking sequences is obtained by shifting top graphene layer along *a*-axis [100] and *b*-axis [010] directions with respect to the bottom layer (fixed). Four corners correspond to configurations with *AB* stackings (Fig. S10 [21]).

of 1.94 and 3.14 Å in ΔPDFs. Compared with diaphite [24], a metastable carbon phase consisting of a mixed sp^2-sp^3 hybridization with various σ-type bond lengths less than ∼2Å, the observed distorted transient diamondlike structure can be treated as a 2D diaphite (named diaphitene).

The crucial role that TBG played in sp^2-sp^3 bond changes can be described mainly from two aspects: stacking sequence and twist angle. To further reveal the role, generalized stacking fault energy (GSFE) surfaces for bilayer graphene with *AB* stacking (Fig. S10 [21]) and the energy surface as a function of rotation angles (Fig. S11 [21]) are evaluated using first-principles calculations under different layer spacings (see the Supplemental Material), respectively. For a stacking sequence, we first obtain a 2D map of bilayer graphene with different stacking sequences (Figs. S10a and S10b [21]) by shifting the top graphene layer along the *a*-axis [100] and the *b*-axis [010] directions with respect to the bottom layer (fixed). For example, as shown in Fig. S10b [21], *AB* stacking is located at four corners: 1/3 of the long diagonal from the upper left corner corresponds to *AA* stacking and 2/3 corresponds to *AC* stacking (*AC* = *AB* in the of bilayer graphene); *AB*′ is at the midpoint of *AC* and *AB* on this diagonal. Three *AB*′ coordinates can be found in the diagram due to the symmetry. Then we calculated the GSFE surfaces for bilayer graphene under different layer spacings [Figs. 4(c)–4(e) and Fig. S10c [21]]. When the layer spacing is larger than 2.4 Å, the bilayer graphene with *AB* stacking (ground state) has the lowest free energy, and, due to the Pauli repulsion, *AA* stacking has the highest free energy. Bilayer graphene with *AB*′ stacking becomes the ground state under compression when the layer spacing is in the range between 2.4 and 2.2 Å. Further compressing layers below ∼2.0 Å changes the ground state to the *AA* stacking, due to the strong covalent effect between overlaying C atoms (formation of sp^3 bonds). This calculation indicates that bilayer graphene with *AA* and *AB*′ stacking is more prone to forming sp^3 bonds than *AB* stacking under compression, which is consistent with the MD simulated structural evolution during compression. In addition, the

potential-energy surface of TBG as a function of the twisted angles shows no significant angle dependence except for the maximum energy at angles of near 0° with *AB* stacking (Fig. S11 [21]). This indicates that the sp^3 bond formation directly from *AB*-stacked graphene sheets has a much higher energy barrier than from TBG. Once the twist angle is away from 0° with *AB* stacking, TBG starts to create a moiré pattern with *AA* and *AB′* stacking configurations which are more prone to forming sp^3 bonds as described above. It is also consistent with numerous theoretical predictions that direct transformation from graphite to diamond must undergo a sliding process to form *AA* stacking and *AB′* stacking. All these observations directly indicate that the moiré pattern of TBG plays an important role in the sp^2-sp^3 transformation.

In conclusion, using ultrafast electron diffraction, we show a diamondlike transient state in TBG under fs laser irradiation. We observe the appearance of bonding distances of 1.94 and 3.14 Å within 330 fs in time-dependent difference pair distribution function identifying a transient 2D diamondlike structure consisting of mixed sp^2 and sp^3 bonds. Such a photoinduced structural transformation is not observed in aligned graphene sheets. On the contrary, the only lattice vibration was detected in aligned graphene sheets under fs laser irradiation. Molecular dynamics and first-principles calculation indicate that the TBG moiré pattern naturally provides stacking configurations like *AA* and *AB′* favorable for the preferential formation of sp^3 bonds. This discovery using TBG offers a promising way to open and precisely tune a band gap in the graphene system, enabling the exploration of innovative applications for the future. This also provides insights into the understanding of the ultrafast optical response of twisted 2D vdW materials. In addition, this work sheds light on the direct graphite-to-diamond transformation mechanism, which has not been fully understood for more than 60 years.

We thank Dr. J. A. Jaszczak for providing single-crystal bulk graphite samples, Dr. M. Harb and Dr. M. Mo for helpful discussion, and S. Yu for assistance in MD simulations. D.L. thanks the China Scholarships Council (CSC) Joint PhD Training Program for the financial support of studying abroad. This work was performed at the Center for Nanoscale Materials, a U.S. Department of Energy Office of Science User Facility, and supported by the US Department of Energy, Office of Science, under Contract No. DE-AC02-06CH11357. The MeV-UED experiments were carried out at SLAC MeV-UED, U.S. Department of Energy Office of Science User Facilities, operated as part of the Linac Coherent Light Source at the SLAC National Accelerator Laboratory, supported by the U.S. Department of Energy, Office of Science, Office of Basic Energy Sciences under Contract No. DE-AC02-76SF00515. This work was also supported by the National Natural Science Foundation of China (NSFC, Grants No. 51925105, No. 51771165, and No. 11805267), and the National Key R&D Program of China (Grant No. YS2018YFA070119).

D.L. and D.H. contributed equally to this work.

[1] S. Carr, D. Massatt, S. Fang, P. Cazeaux, M. Luskin, and E. Kaxiras, Phys. Rev. B **95**, 075420 (2017).

[2] Y. Cao, V. Fatemi, S. Fang, K. Watanabe, T. Taniguchi, E. Kaxiras, and P. Jarillo-Herrero, Nature (London) **556**, 43 (2018).

[3] M. Yankowitz, S. Chen, H. Polshyn, Y. Zhang, K. Watanabe, T. Taniguchi, D. Graf, A. F. Young, and C. R. Dean, Science **363**, 1059 (2019).

[4] Y. Cao, V. Fatemi, A. Demir, S. Fang, S. L. Tomarken, J. Y. Luo, J. D. Sanchez-Yamagishi, K. Watanabe, T. Taniguchi, and E. Kaxiras, Nature (London) **556**, 80 (2018).

[5] K. Tran, G. Moody, F. Wu, X. Lu, J. Choi, K. Kim, A. Rai, D. A. Sanchez, J. Quan, and A. Singh, Nature (London) **567**, 71 (2019).

[6] C. Jin, E. C. Regan, A. Yan, M. I. B. Utama, D. Wang, S. Zhao, Y. Qin, S. Yang, Z. Zheng, and S. Shi, Nature (London) **567**, 76 (2019).

[7] E. M. Alexeev, D. A. Ruiz-Tijerina, M. Danovich, M. J. Hamer, D. J. Terry, P. K. Nayak, S. Ahn, S. Pak, J. Lee, and J. I. Sohn, Nature (London) **567**, 81 (2019).

[8] K. L. Seyler, P. Rivera, H. Yu, N. P. Wilson, E. L. Ray, D. G. Mandrus, J. Yan, W. Yao, and X. Xu, Nature (London) **567**, 66 (2019).

[9] Y. Jiang, X. Lai, K. Watanabe, T. Taniguchi, K. Haule, J. Mao, and E. Y. Andrei, Nature (London) **573**, 91 (2019).

[10] Y. Xie, B. Lian, B. Jäck, X. Liu, C.-L. Chiu, K. Watanabe, T. Taniguchi, B. A. Bernevig, and A. Yazdani, Nature (London) **572**, 101 (2019).

[11] A. Kerelsky, L. J. McGilly, D. M. Kennes, L. Xian, M. Yankowitz, S. Chen, K. Watanabe, T. Taniguchi, J. Hone, and C. Dean, Nature (London) **572**, 95 (2019).

[12] M. V. Shugaev, C. Wu, O. Armbruster, A. Naghilou, N. Brouwer, D. S. Ivanov, T. J.-Y. Derrien, N. M. Bulgakova, W. Kautek, and B. Rethfeld, MRS Bull. **41**, 960 (2016).

[13] L. Britnell, R. Ribeiro, A. Eckmann, R. Jalil, B. Belle, A. Mishchenko, Y.-J. Kim, R. Gorbachev, T. Georgiou, and S. Morozov, Science **340**, 1311 (2013).

[14] X. Liu, T. Galfsky, Z. Sun, F. Xia, E.-C. Lin, Y.-H. Lee, S. Kéna-Cohen, and V. M. Menon, Nat. Photon. **9**, 30 (2015).

[15] C. Schneider, M. M. Glazov, T. Korn, S. Höfling, and B. Urbaszek, Nat. Commun. **9**, 2695 (2018).

[16] B. Peng, H. Zhang, W. Chen, B. Hou, Z.-J. Qiu, H. Shao, H. Zhu, B. Monserrat, D. Fu, H. Weng, and C. M. Soukoulis, npj 2D Mater. Appl. **4**, 14 (2020).

[17] T. Ishikawa, S. A. Hayes, S. Keskin, G. Corthey, M. Hada, K. Pichugin, A. Marx, J. Hirscht, K. Shionuma, and K. Onda, Science **350**, 1501 (2015).

[18] S. Scandolo, M. Bernasconi, G. L. Chiarotti, P. Focher, and E. Tosatti, Phys. Rev. Lett. **74**, 4015 (1995).

[19] J. Sung, J. Mater. Sci. **35**, 6041 (2000).

[20] X. Dong, X.-F. Zhou, G.-R. Qian, Z. Zhao, Y. Tian, and H.-T. Wang, J. Phys.: Condens. Matter **25**, 145402 (2013).

[21] See Supplemental Material at http://link.aps.org/supplemental/10.1103/PhysRevB.102.155431 for additional methods, calculations, data and fits, which includes Refs. [28,30,42–59].

[22] T. Sano, K. Takahashi, O. Sakata, M. Okoshi, N. Inoue, K. F. Kobayashi, and A. Hirose, J. Phys. Conf. Ser. **165**, 012019 (2009).

[23] R. Nüske, A. Jurgilaitis, H. Enquist, M. Harb, Y. Fang, U. Håkanson, and J. Larsson, Appl. Phys. Lett. **100**, 043102 (2012).

[24] J. Kanasaki, E. Inami, K. Tanimura, H. Ohnishi, and K. Nasu, Phys. Rev. Lett. **102**, 087402 (2009).

[25] R. K. Raman, Y. Murooka, C.-Y. Ruan, T. Yang, S. Berber, and D. Tománek, Phys. Rev. Lett. **101**, 077401 (2008).

[26] F. Carbone, O.-H. Kwon, and A. H. Zewail, Science **325**, 181 (2009).

[27] F. Carbone, P. Baum, P. Rudolf, and A. H. Zewail, Phys. Rev. Lett. **100**, 035501 (2008).

[28] S. Schäfer, W. Liang, and A. H. Zewail, New J. Phys. **13**, 063030 (2011).

[29] R. P. Chatelain, V. R. Morrison, B. L. M. Klarenaar, and B. J. Siwick, Phys. Rev. Lett. **113**, 235502 (2014).

[30] M. Harb, H. Enquist, A. Jurgilaitis, F. Tuyakova, A. N. Obraztsov, and J. Larsson, Phys. Rev. B **93**, 104104 (2016).

[31] M. J. Stern, L. P. R. de Cotret, M. R. Otto, R. P. Chatelain, J.-P. Boisvert, M. Sutton, and B. J. Siwick, Phys. Rev. B **97**, 165416 (2018).

[32] J. Hu, G. M. Vanacore, A. Cepellotti, N. Marzari, and A. H. Zewail, Proc. Natl. Acad. Sci. USA **113**, E6555 (2016).

[33] S. Schäfer, W. Liang, and A. H. Zewail, Chem. Phys. Lett. **493**, 11 (2010).

[34] H. Park and J.-M. Zuo, Phys. Rev. Lett. **105**, 059603 (2010).

[35] H. Park and J. Zuo, Appl. Phys. Lett. **94**, 251103 (2009).

[36] Materials science: Diaphite domains. Nature (London) **458**, 129 (2009).

[37] J. C. Meyer, A. Geim, M. Katsnelson, K. Novoselov, D. Obergfell, S. Roth, C. Girit, and A. Zettl, Solid State Commun. **143**, 101 (2007).

[38] N. Mounet and N. Marzari, Phys. Rev. B **71**, 205214 (2005).

[39] J. Yang, X. Zhu, T. J. Wolf, Z. Li, J. P. F. Nunes, R. Coffee, J. P. Cryan, M. Gühr, K. Hegazy, and T. F. Heinz, K. Jobe, R. Li, X. Shen, T. Veccione, S. Weathersby, K. J. Wilkin, C. Yoneda, Q. Zheng, T. J. Martinez, M. Centurion, and X. Wang, Science **361**, 64 (2018).

[40] A. Burian, J. C. Dore, and K. Jurkiewicz, Rep. Prog. Phys. **82**, 016501 (2018).

[41] N. Woznica, L. Hawelek, H. E. Fischer, I. Bobrinetskiy, and A. Burian, J. Appl. Crystallogr. **48**, 1429 (2015).

[42] S. Weathersby, G. Brown, M. Centurion, T. Chase, R. Coffee, J. Corbett, J. Eichner, J. Frisch, A. Fry, and M. Gühr, Mega-electron-volt ultrafast electron diffraction at SLAC national accelerator laboratory, Rev. Sci. Instrum. **86**, 073702 (2015).

[43] X. Shen, R. Li, U. Lundström, T. Lane, A. Reid, S. Weathersby, and X. Wang, Femtosecond mega-electron-volt electron microdiffraction, Ultramicroscopy **184**, 172 (2018).

[44] K. S. Novoselov, A. K. Geim, S. V. Morozov, D. Jiang, Y. Zhang, S. V. Dubonos, I. V. Grigorieva, and A. A. Firsov, Electric field effect in atomically thin carbon films, Science **306**, 666 (2004).

[45] X. Wu, L. Z. Tan, X. Shen, T. Hu, K. Miyata, M. T. Trinh, R. Li, R. Coffee, S. Liu, and D. A. Egger, Light-induced picosecond rotational disordering of the inorganic sublattice in hybrid perovskites, Sci. Adv. **3**, e1602388 (2017).

[46] F. Salvat, A. Jablonski, and C. J. Powell, ELSEPA—Dirac partial-wave calculation of elastic scattering of electrons and positrons by atoms, positive ions and molecules, Comput. Phys. Commun. **165**, 157 (2005).

[47] V. Vítek, Intrinsic stacking faults in body-centred cubic crystals, Philos. Mag. **18**, 773 (1968).

[48] G. Kresse and J. Furthmüller, Efficient iterative schemes for ab initio total-energy calculations using a plane-wave basis set, Phys. Rev. B **54**, 11169 (1996).

[49] J. P. Perdew and A. Zunger, Self-interaction correction to density-functional approximations for many-electron systems, Phys. Rev. B **23**, 5048 (1981).

[50] G. Kresse and D. Joubert, From ultrasoft pseudopotentials to the projector augmented-wave method, Phys. Rev. B **59**, 1758 (1999).

[51] S. Plimpton, Fast parallel algorithms for short-range molecular dynamics, J. Comput. Phys. **117**, 1 (1995).

[52] A. Stukowski, Visualization and analysis of atomistic simulation data with OVITO-the Open Visualization Tool, Model. Simul. Mater. Sci. **18**, 015012 (2009).

[53] A. C. Van Duin, S. Dasgupta, F. Lorant, and W. A. Goddard, ReaxFF: a reactive force field for hydrocarbons, J. Phys. Chem. A **105**, 9396 (2001).

[54] T.-R. Shan and A. P. Thompson J. Phys.: Conf. Ser. **500**, 172009 (2014).

[55] C. Gerbig, A. Senftleben, S. Morgenstern, C. Sarpe, and T. Baumert, Spatio-temporal resolution studies on a highly compact ultrafast electron diffractometer, New J. Phys. **17**, 043050 (2015).

[56] V. K. Tewary and B. Yang, Singular behavior of the Debye-Waller factor of graphene, Phys. Rev. B **79**, 125416 (2009).

[57] I. Giordanelli, M. Mendoza, and H. J. Herrmann, Modelling electron-phonon interactions in graphene with curved space hydrodynamics, Sci. Rep. **8**, 12545 (2018).

[58] D. K. Efetov and P. Kim, Controlling Electron-Phonon Interactions in Graphene at Ultrahigh Carrier Densities, Phys. Rev. Lett. **105**, 256805 (2010).

[59] E. Pop, V. Varshney, and A. K. Roy, Thermal properties of graphene: Fundamentals and applications, MRS Bull. **37**, 1273 (2012).